European Radiology (2019) 29:4861–4870
https://doi.org/10.1007/s00330-019-06114-x

UROGENITAL

Correlation between MRI phenotypes and a genomic classifier of prostate cancer: preliminary findings

Andrei S. Purysko[1] · Cristina Magi-Galluzzi[2] · Omar Y. Mian[3] · Sarah Sittenfeld[3] · Elai Davicioni[4] · Marguerite du Plessis[4] · Christine Buerki[4] · Jennifer Bullen[5] · Lin Li[6] · Anant Madabhushi[6] · Andrew Stephenson[7] · Eric A. Klein[7]

Received: 20 December 2018 / Revised: 7 February 2019 / Accepted: 15 February 2019 / Published online: 7 March 2019

Abstract

Objectives We sought to evaluate the correlation between MRI phenotypes of prostate cancer as defined by PI-RADS v2 and the Decipher Genomic Classifier (used to estimate the risk of early metastases).

Methods This single-center, retrospective study included 72 nonconsecutive men with prostate cancer who underwent MRI before radical prostatectomy performed between April 2014 and August 2017 and whose MRI registered lesions were micro-dissected from radical prostatectomy specimens and then profiled using Decipher (89 lesions; 23 MRI invisible [PI-RADS v2 scores ≤ 2] and 66 MRI visible [PI-RADS v2 scores ≥ 3]). Linear regression analysis was used to assess clinicopathologic and MRI predictors of Decipher results; correlation coefficients (r) were used to quantify these associations. AUC was used to determine whether PI-RADS v2 could accurately distinguish between low-risk (Decipher score < 0.45) and intermediate-/high-risk (Decipher score ≥ 0.45) lesions.

Results MRI-visible lesions had higher Decipher scores than MRI-invisible lesions (mean difference 0.22; 95% CI 0.13, 0.32; $p < 0.0001$); most MRI-invisible lesions (82.6%) were low risk. PI-RADS v2 had moderate correlation with Decipher ($r = 0.54$) and had higher accuracy (AUC 0.863) than prostate cancer grade groups (AUC 0.780) in peripheral zone lesions (95% CI for difference 0.01, 0.15; $p = 0.018$).

Conclusions MRI phenotypes of prostate cancer are positively correlated with Decipher risk groups. Although PI-RADS v2 can accurately distinguish between lesions classified by Decipher as low or intermediate/high risk, some lesions classified as intermediate/high risk by Decipher are invisible on MRI.

Key Points

- *MRI phenotypes of prostate cancer as defined by PI-RADS v2 positively correlated with a genomic classifier that estimates the risk of early metastases.*
- *Most but not all MRI-invisible lesions had a low risk for early metastases according to the genomic classifier.*
- *MRI could be used in conjunction with genomic assays to identify lesions that may carry biological potential for early metastases.*

Electronic supplementary material The online version of this article (https://doi.org/10.1007/s00330-019-06114-x) contains supplementary material, which is available to authorized users.

✉ Andrei S. Purysko
puryska@ccf.org

[1] Abdominal Imaging Section and Nuclear Radiology Department, Imaging Institute, Cleveland Clinic, 9500 Euclid Ave, Cleveland, OH 44195, USA

[2] Pathology and Laboratory Medicine Institute, Cleveland Clinic, 9500 Euclid Ave, Cleveland, OH 44195, USA

[3] Radiation Oncology and Translational Oncology, Cleveland Clinic, 9500 Euclid Ave, Cleveland, OH 44195, USA

[4] GenomeDx Biosciences, Vancouver, BC, Canada

[5] Quantitative Health Sciences, Cleveland Clinic, 9500 Euclid Ave, Cleveland, OH 44195, USA

[6] Department of Biomedical Engineering, Case Western Reserve University, Cleveland, OH, USA

[7] Glickman Urological and Kidney Institute, Cleveland Clinic, 9500 Euclid Ave, Cleveland, OH 44195, USA

Keywords Prostatic neoplasms · Magnetic resonance imaging · Genes

Abbreviations

GG	Grade group
GS	Gleason score
H&E	Hematoxylin and eosin
PCa	Prostate cancer
PZ	Peripheral zone
RP	Radical prostatectomy
TZ	Transition zone

Introduction

Despite a recent decline in incidence, prostate cancer (PCa) remains the most common solid noncutaneous cancer in men in the USA [1]. The American Cancer Society estimates that in 2018, a total of 29,430 men will die as a result of this disease [1]. Conversely, many PCa cases are indolent and may not require any treatment [2]. Thus, stratification of the potential risks for metastatic progression and prostate cancer-specific mortality is a critical step in the management of PCa. This stratification has traditionally relied on clinicopathologic features such as serum prostate-specific antigen (PSA) level, clinical stage, and Gleason score (GS). Recently, however, several molecular profiling assays have been developed and are increasingly being utilized for risk stratification [2, 3]. The Decipher Genomic Classifier is one such assay that relies on tumor gene expression profiling to distinguish aggressive PCa based on its molecular features and thus predict the occurrence of early metastases after radical prostatectomy (RP) [4–6].

In the pretreatment setting, prostate MRI appears to offer high accuracy in detecting clinically significant cases of PCa (i.e., GS ≥ 3 + 4) [7–9]; however, MRI does not detect all clinically significant tumors and sometimes cannot differentiate between these tumors and benign conditions such as prostatitis or benign prostatic hyperplasia [10–13]. These undetected tumors are commonly said to be "MRI invisible."

Preliminary studies have suggested that the MRI phenotypes of PCa have prognostic implications [13–16]. To fully understand the significance of these MRI phenotypes, we must evaluate their risk for progression and metastases based on correlation not only with clinicopathologic features but also with the expression of genes that confer a biological potential for aggressiveness. The aim of this study was therefore to evaluate the correlation between the Decipher Genomic Classifier score and the MRI phenotype of PCa as defined by the PI-RADS v2 scoring system in men who had undergone RP.

Materials and methods

The local Institutional Review Board waived the need for written informed consent due to the minimal risk and retrospective nature of this study.

Eligibility criteria for study patients included a history of PCa treated with RP but with no preoperative neoadjuvant treatment, availability of preoperative MR images of the prostate using PI-RADS v2 technical standards [17] and demonstrating adequate image quality, and availability of RP specimens for direct radiologic and pathologic correlation.

Cases considered for inclusion were identified from two sources (Fig. 1). First, we reviewed the records from 56 patients with PCa who underwent RP at a single institution between April 2014 and January 2015 and whose RP specimens were interpreted by a single genitourinary pathologist with 15 years' experience (C.M.-G.). The first 35 consecutive patients who met the eligibility criteria were included in the study (group 1). The second source was an institutional database of patients with PCa who underwent Decipher testing as part of their clinical care after their RP specimens were found to have high-risk features for progression (e.g., extraprostatic extension, seminal vesicle invasion, positive surgical margin). Among 166 patients identified through this search, 37 (RP performed between April 2014 and August 2017) met the eligibility criteria and were included in the study (group 2). Our final cohort therefore included a total of 72 patients (Table 1).

Multiparametric MRI protocol and interpretation

All scans were performed on a 3-T MR scanner (Magnetom Skyra; Siemens) without an endorectal coil (acquisition parameters presented in Supplemental Table). MR images were retrospectively interpreted by a single reader with 8 years' experience with prostate MRI (A.S.P.) who was initially blinded to the clinicopathologic information. On MRI, the index lesion was considered the lesion with the highest PI-RADS v2 score [17]. If more than one lesion with the same PI-RADS v2 score was present, the index lesion was the one that showed extraprostatic extension. If none of the lesions demonstrated extraprostatic extension, the largest of the lesions with the highest score was considered the index lesion.

Histopathologic analysis

All RP specimens were weighed, inked, fixed in formalin, and serially sectioned at 3-mm intervals. The prostate slices were subdivided in quadrants and labeled to allow for reconstruction as whole-mount sections. Prostate tissue sections were embedded in paraffin, and a 4-μm section from each block was stained with

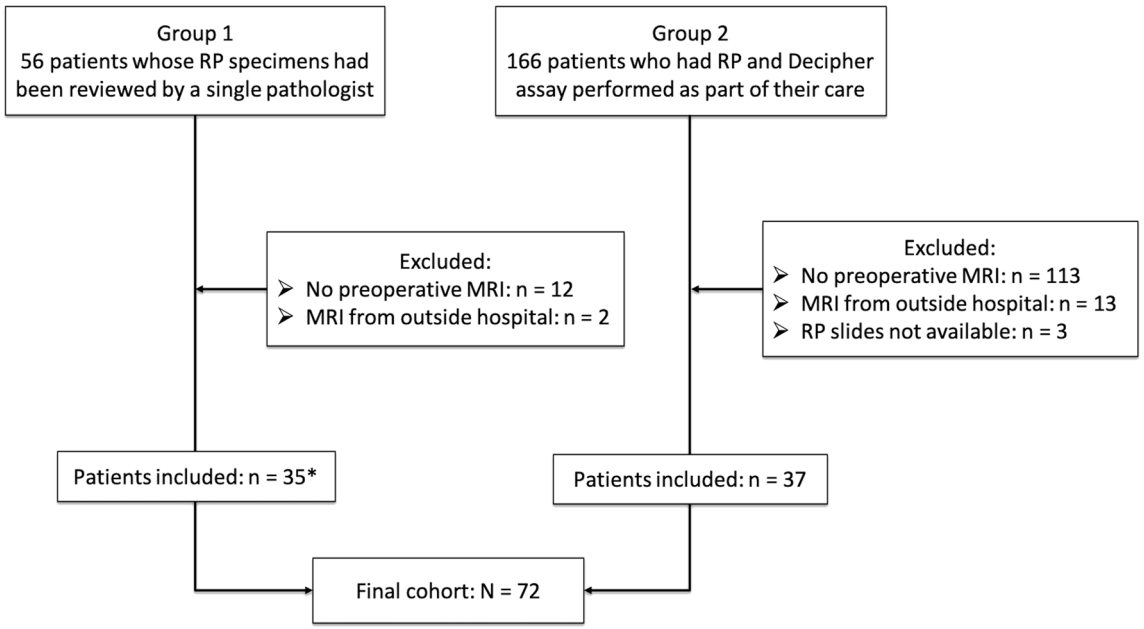

Fig. 1 Study flowchart. *First 35 consecutive patients who met eligibility criteria

hematoxylin and eosin (H&E). The genitourinary pathologist annotated all tumor foci in each H&E slide and created RP maps indicating the location and morphologic features of all tumors, GS and corresponding grade group (GG), pathologic stage, and surgical margin status. The glass slides were then scanned (Aperio AT Turbo Digital scanner; Leica Biosystems) at ×20 magnification, and a free software program (AutoStitcher [18]) was used to merge the quadrants together, simulating the appearance of a whole-mount specimen.

MRI and pathology correlation

After MR images were initially interpreted, the pathologist disclosed the RP maps to the radiologist, and the radiologist and pathologist jointly determined whether a tumor on the RP maps had a corresponding lesion on the MR images. Lesions with a PI-RADS v2 score of 3, 4, or 5 and with corresponding tumors on the RP maps were considered MRI visible; tumors that were present on the RP maps but did not appear as a

Table 1 Clinicopathologic information

Clinicopathologic characteristic	Group 1 ($n = 35$)	Group 2 ($n = 37$)	Combined cohort ($N = 72$)
Age (years)*	61 ± 7 (42–76)	64 ± 7 (42–75)	63 ± 7 (42–76)
Preoperative PSA (ng/mL)*	6.0 ± 5 (1.2–26)	13.4 ± 15 (2.1–69)	9.8 ± 12 (1.2–69)
Interval between MRI and RP (days)†	65 ± 32 [7, 146]	51 ± 56 [0, 284]	58 ± 46 [0, 284]
Prostate cancer grade group			
1	1 (3)	0 (0)	1 (1)
2	22 (63)	9 (24)	31 (43)
3	8 (23)	9 (24)	17 (24)
4	2 (6)	4 (11)	6 (8)
5	2 (6)	15 (41)	17 (24)
Extraprostatic extension	11 (31)	34 (92)	45 (63)
Seminal vesicle invasion	1 (3)	15 (41)	16 (22)
Lymphovascular space invasion	3 (9)	17 (53)‡	20 (30)‡
Positive surgical margin	13 (37)	24 (65)	37 (51)

Unless otherwise indicated, data are numbers of patients, and data in parentheses are percentages

PSA prostate-specific antigen, *RP* radical prostatectomy

*Data are mean ± standard deviation, and data in parentheses are ranges

†Data are mean ± standard deviation, and data in brackets are ranges

‡Status unknown for five patients

corresponding focal lesion on the MR images after the RP maps were disclosed to the radiologist were considered MRI invisible and received a PI-RADS v2 score of 1 or 2. MR images and the annotated digitized RP images were then coregistered using a multiscale spectral embedding registration technique [19] to ensure that the tumors were correctly located on the MR images (Fig. 2).

Tissue sampling and molecular assay

For group 1, tissue samples were obtained from the blocks corresponding to the location of the index MRI-visible tumor and from up to two additional MRI-visible or MRI-invisible tumors separate from the index tumor. If no MRI-visible tumor was identified, up to two MRI-invisible tumors were sampled per patient. For group 2, only the tumor with the highest GS was sampled, as per clinical protocol. These samples were obtained using a 2 × 0.6-mm biopsy punch tool. The tissue cores were placed in a microfuge tube for processing. Subsequently, RNA extraction and microarray expression data generation were performed. The Decipher molecular assay was performed in a CAP/CLIA laboratory (GenomeDx Biosciences) as previously described [6].

The Decipher Genomic Classifier consists of 22 RNA-expression–based genomic markers that are involved in PCa pathogenesis and relate to cellular differentiation, cellular adhesion and motility, cell cycle progression, androgen signaling, and immune modulation. The Decipher Genomic Classifier provides a continuous risk score between 0 and 1, with higher scores indicating a higher risk of metastases and PCa-related death. For this study, we used previously established cutoff points to categorize lesions as low risk (score < 0.45), intermediate risk (score of 0.45–0.60), or high risk (score > 0.60) [4–6]. In clinical practice, the Decipher Genomic Classifier is used to stratify the aforementioned risk in patients with adverse pathology after RP. Decipher low-risk patients have an excellent prognosis with salvage radiation and may not require concurrent hormonal therapy because the incidence of metastasis remains low. On the other hand, Decipher high-risk patients may require intensification of therapy beyond radiation because the incidence of metastasis remains high [20].

Statistical analysis

At the lesion level, the lesion's Decipher risk group was used as the primary outcome. Ordinal logistic regression models were used to individually assess the following potential predictors: PI-RADS v2 scores, MRI visibility (MRI visible vs MRI invisible), index status (index lesion vs nonindex lesion), lesion location (peripheral zone [PZ] vs transition zone [TZ]), and GG. In all lesion-level models, generalized estimating equations were used to estimate model parameters to account for the clustered nature of the data (multiple lesions per patient). Spearman's correlation coefficient (r) was used to

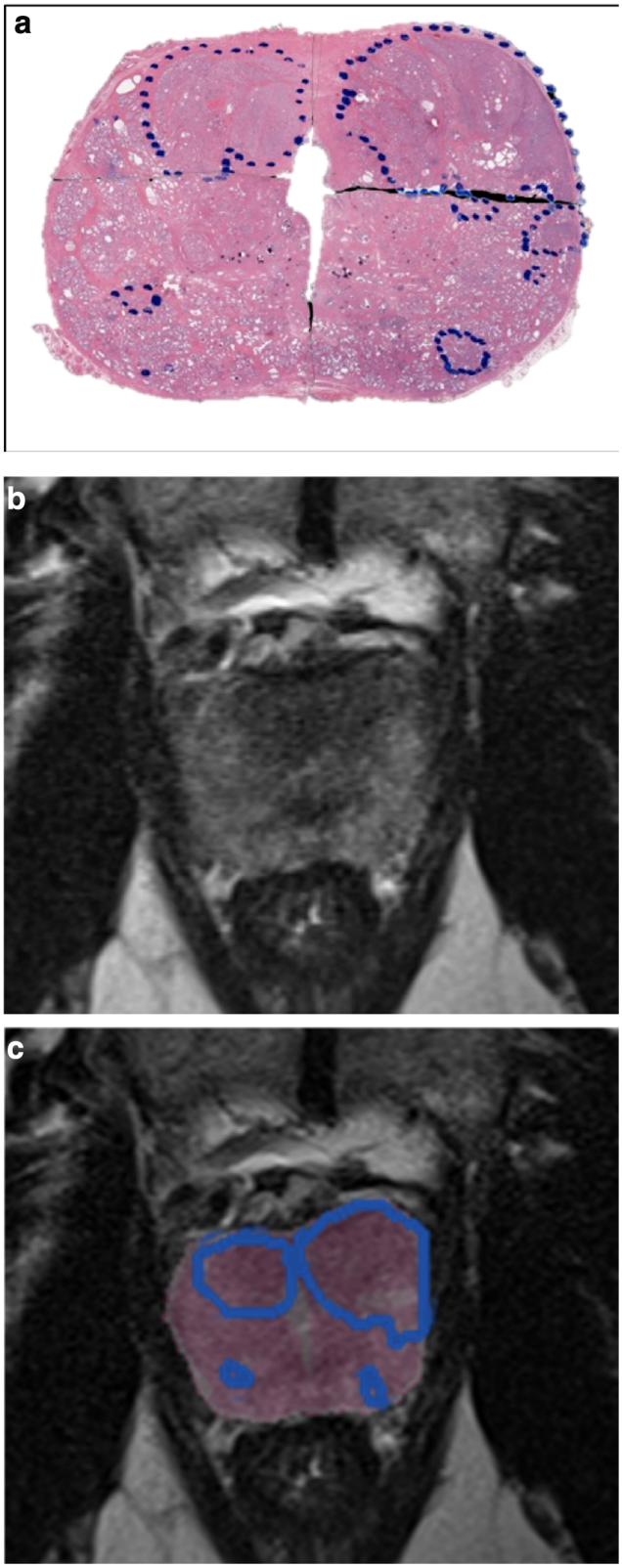

Fig. 2 Coregistration of pathological and MR images. **a** Digitally reconstructed whole-mount RP specimen from H&E-stained slides at the prostate apex with tumor annotations (dotted regions). **b** Axial T2 turbo spin-echo image at the corresponding level. **c** RP image with annotated tumor foci overlaying the T2-weighted image

Table 2 PI-RADS v2 scores and Decipher risk groups for 89 lesions

MRI visibility	PI-RADS v2 score	Decipher Genomic Classifier group		
		Low risk (< 0.45) ($n = 41$)	Intermediate risk (0.45–0.60) ($n = 12$)	High risk (> 0.60) ($n = 36$)
MRI invisible ($n = 23$)	1 ($n = 11$)	9	1*	1†
	2 ($n = 12$)	10	2‡	0
MRI visible ($n = 66$)	3 ($n = 4$)	4	0	0
	4 ($n = 15$)	7	2	6
	5 ($n = 47$)	11	7	29

*Grade group (GG) 1 tumor. Patient had a GG 3 tumor with a PI-RADS v2 score of 5 in a different location that was low risk (0.32)

†GG 1 tumor with a Decipher score of 0.67. Patient also had a GG 3 tumor with a PI-RADS v2 score of 5 and a Decipher score of 0.79

‡GG 1 and GG 2 tumors in distinct patients who had no other lesions with PI-RADS v2 scores of 3–5

characterize the amount of rank correlation between each potential predictor and the lesion's Decipher risk group. An unpaired *t* test was used to compare the mean Decipher scores of MRI-visible and MRI-invisible lesions, MRI index and nonindex lesions, and PZ and TZ lesions. The receiver operating characteristic curve was used to characterize the accuracy with which PI-RADS v2 scores could be used to distinguish lesions with low risk (Decipher score < 0.45) from those with intermediate/high risk (Decipher score ≥ 0.45). The AUC was estimated using nonparametric methods. The AUC of PI-RADS v2 scores was compared to the AUC of GG using methods that accounted for the clustered nature of the data [21]. A type 1 error rate of less than 0.05 was considered significant for all analyses.

Results

Lesion characteristics

The Decipher Genomic Classifier was used for 89 lesions (single lesion in 56 patients, 2 lesions in 15 patients, and 3 lesions in 1 patient); 52 lesions were sampled from group 1 and 37 lesions were sampled from group 2 (Tables 2 and 3). Most lesions sampled were located in the PZ ($n = 72$ [81%]) and were index lesions ($n = 70$ [78.6%]). In 96.7% (59/61) of the patients who had at least one MRI-visible tumor, the index lesion on MRI corresponded to the lesion with the highest GG on histopathology. No MRI-visible lesions were identified in 15.3% (11/72) of patients. In this group of patients without MRI-visible lesions, PCa was detected by systematic 12-core transrectal ultrasound-guided biopsy.

Correlation between lesion characteristics and Decipher scores

Associations between lesion characteristics and each lesion's Decipher score and risk group are shown in Table 4 and Fig. 3. The mean Decipher score for MRI-visible lesions (0.58 ± 0.21; range 0.04–0.93) was significantly higher than the mean Decipher score for MRI-invisible lesions (0.35 ± 0.14; range 0.09–0.67) (mean difference 0.22; 95% CI 0.13, 0.32; $p < 0.0001$). Among the 23 MRI-invisible lesions, 19 (82.6%) were low risk, 3 (13%) were intermediate risk, and 1 (4.4%) was high risk (Table 2). Among the three patients with MRI-invisible lesions that were considered intermediate risk, one patient also had an MRI-visible lesion that was low risk; the other two patients had no MRI-visible lesions. The one patient with an MRI-invisible lesion that was classified as high risk (Decipher score 0.67; GG 1) also had a separate

Table 3 MRI visibility and prostate cancer grade group for 89 lesions

MRI visibility	PI-RADS v2 score	Grade group				
		1 ($n = 8$)	2 ($n = 40$)	3 ($n = 18$)	4 ($n = 5$)	5 ($n = 18$)
MRI invisible ($n = 23$)	1 ($n = 11$)	4	7	0	0	0
	2 ($n = 12$)	3	8	1	0	0
MRI visible ($n = 66$)	3 ($n = 4$)	0	4	0	0	0
	4 ($n = 15$)	0	10	2	2	1
	5 ($n = 47$)	1	11	15	3	17

Table 4 Association between various lesion characteristics and Decipher risk group

Lesion characteristic	Correlation with Decipher risk group	
	r	*p* value
PI-RADS v2 score in all lesions	0.54	< 0.001
PI-RADS v2 score in PZ lesions	0.67	< 0.001
MR visibility	0.46	< 0.001
Index status	0.38	< 0.001
Location	0.16	0.207
Grade group	0.47	< 0.001

PZ peripheral zone

ipsilateral MRI-visible tumor (PI-RADS v2 score of 5; GG 3) with a higher Decipher score (0.79) (Fig. 4).

The mean Decipher score for PZ lesions (0.54 ± 0.21; range 0.09–0.93) was significantly higher than the mean Decipher score for TZ lesions (0.42 ± 0.22; range 0.04–0.80) (mean difference 0.12; 95% CI 0.01, 0.24; $p = 0.034$). However, the correlation between lesion location (PZ vs TZ) and Decipher risk group was not significant ($p = 0.207$; Table 4).

PI-RADS v2 score was positively correlated with the Decipher risk group ($r = 0.54$; $p < 0.001$). This correlation was stronger for lesions located in the PZ ($r = 0.67$; $p < 0.001$; Table 4). The partial correlation between PI-RADS v2 score and Decipher group after adjustments were made for GG was 0.35 ($p = 0.001$). The correlation between PI-RADS v2 and Decipher risk group was significantly different between index lesions and nonindex lesions (interaction $p < 0.001$). For index lesions, a higher PI-RADS v2 score was associated with a higher Decipher risk group ($r = 0.47$). However, for nonindex lesions, a higher PI-RADS v2 score was not necessarily associated with a higher Decipher risk group ($r = 0.04$). Among the 16 patients with more than one lesion sampled, the Decipher risk group for index lesions versus nonindex lesions was higher in 7 patients (43.7%), equal in 7 patients (43.7%), and lower in 2 patients (12.5%).

In distinguishing between Decipher low-risk and intermediate-/high-risk lesions, the AUC for PI-RADS v2 score (0.776) was slightly higher than the AUC for GG (0.739) (95% CI for difference − 0.06, 0.13; $p = 0.446$) (Fig. 5). For lesions located in the PZ only, the AUC for PI-RADS v2 scores (0.863) was significantly higher than the AUC for GG (0.780) (95% CI for difference 0.01, 0.15; $p = 0.018$).

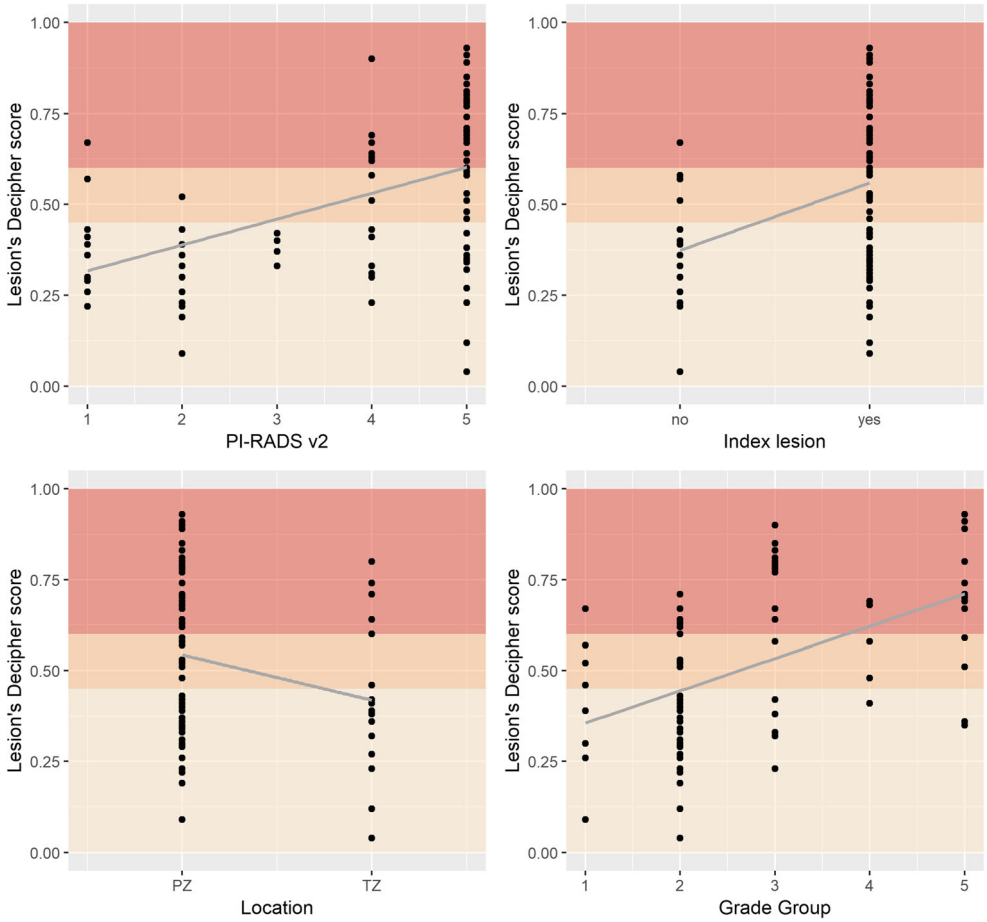

Fig. 3 Relationship between various lesion characteristics and each lesion's Decipher score. Decipher risk groups are shaded light red for low risk, medium red for medium risk, and dark red for high risk. The gray line represents the best fit line from a simple linear regression (fit using ordinary least squares)

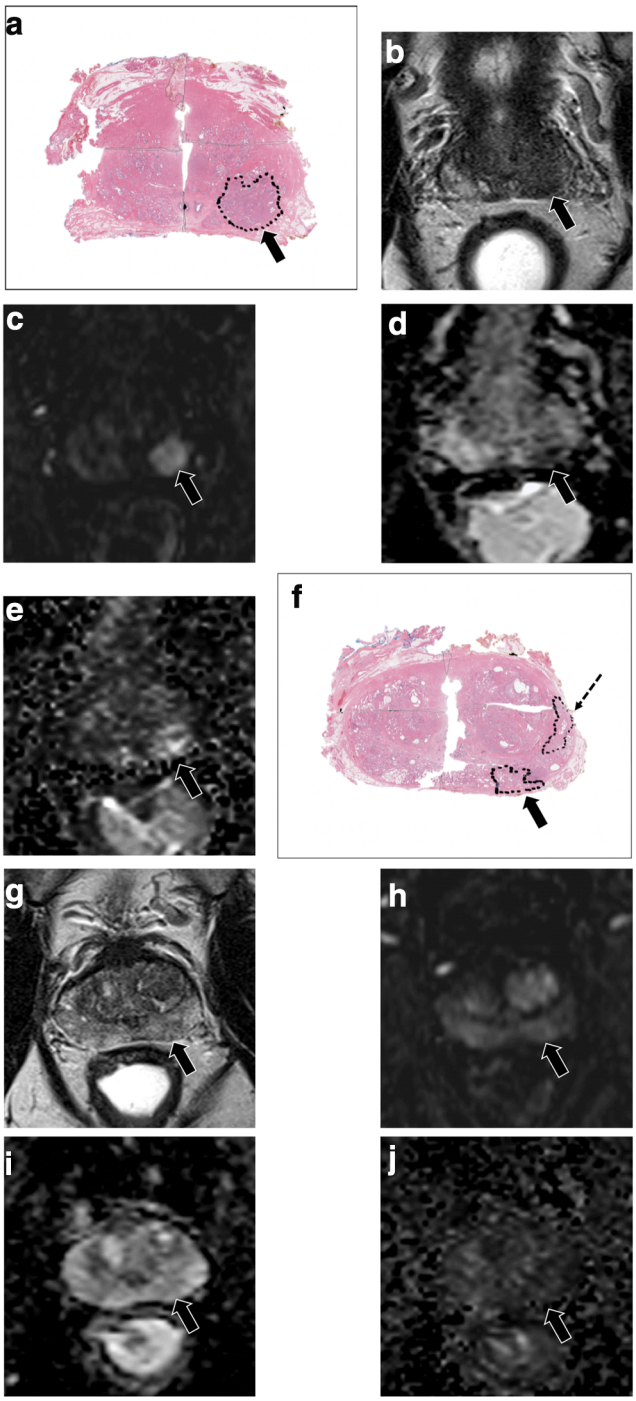

Fig. 4 A 59-year-old man presented with MRI-visible and MRI-invisible prostate tumors. **a** Digitally reconstructed whole-mount RP specimen from H&E-stained slides of the prostate base shows a GG 3 tumor (arrow) centered in the left PZ. **b** Axial 2D turbo spin-echo T2-weighted image shows a corresponding focal lesion measuring 1.6 cm with low signal intensity (arrow). **c** The lesion demonstrates early arterial enhancement on the axial dynamic contrast-enhanced T1-weighted image (arrow). **d**, **e** The lesion demonstrates markedly low signal intensity on the axial apparent diffusion coefficient map (arrow) and markedly high signal intensity on the axial high *b*-value (calculated 1500 s/mm^2) diffusion-weighted image (arrow). The lesion was categorized as PI-RADS v2 5 with a Decipher risk score of 0.79 (i.e., high risk). **f** Digitally reconstructed whole-mount RP specimen from H&E-stained slides at the mid gland level shows two distinct GG 1 nonindex tumors in the left posteromedial (solid arrow) and posterolateral (dashed arrow) PZ. **g** Axial 2D turbo spin-echo T2-weighted image shows mild diffuse low signal in the PZ (arrow) but no corresponding focal lesions. **h** There is diffuse early arterial enhancement on the axial dynamic contrast-enhanced T1-weighted image (arrow). **i**, **j** Indistinct hypointense signal can be seen on the axial apparent diffusion coefficient map (arrow), with no focal lesions with hyperintense signal on the axial high *b*-value (calculated 1500 s/mm^2) diffusion-weighted image (arrow). The PI-RADS v2 assessment category was 2. The lesion in the posteromedial PZ was microdissected and had a Decipher risk score of 0.67 (i.e., high risk)

Discussion

In this study, we found that MRI-visible tumors were associated with significantly higher Decipher scores than MRI-invisible tumors. Additionally, we found that most MRI-invisible lesions had low risk for metastasis as determined by the Decipher assay, a well-validated predictor of oncologic outcomes [22–26].

Although MRI visibility has traditionally been attributed to histologic features of PCa, emerging data suggest that these may not be the only factors involved. In a differential gene expression analysis of GS and tumor volume, investigators found that despite some overlap, genes associated with tumor volume and GS were different from a subset of genes associated with MRI visibility, suggesting that MRI visibility is not fully explained by variability in GS or tumor volume [27]. The authors also conducted an experiment using xenografts in mice in which genes associated with both MRI visibility and poor prognosis were suppressed, resulting in tumors with decreased visibility on diffusion-weighted imaging and decreased perfusion. In a recent retrospective study using genome-wide expression analysis in 206 patients with PCa who underwent RP, signaling pathways associated with adverse pathological outcomes such as cell cycle progression (PI3K-AKT-mTOR and E2F) and castration resistance (WNT-b) were found to be more active in lesions with a PI-RADS v2 score of 5 than in those with scores of 3 or 4 [28]. A significant association between PI-RADS v2 and Decipher scores was also observed, although only MRI-visible lesions (i.e., PI-RADS v2 scores 3–5) were included in this study.

In our study, most of the MRI-visible index lesions corresponded to lesions with the highest GG and were classified as higher risk versus nonindex lesions on Decipher testing. Although a positive correlation was observed between PI-RADS v2 scores of index lesions and their Decipher risk groups, there was no such significant correlation in nonindex lesions. In a previous retrospective analysis of seven patients with PCa who underwent MRI-guided biopsy before RP, researchers observed an 83% concordance of Decipher risk groups in tissue obtained from index lesions in biopsies and

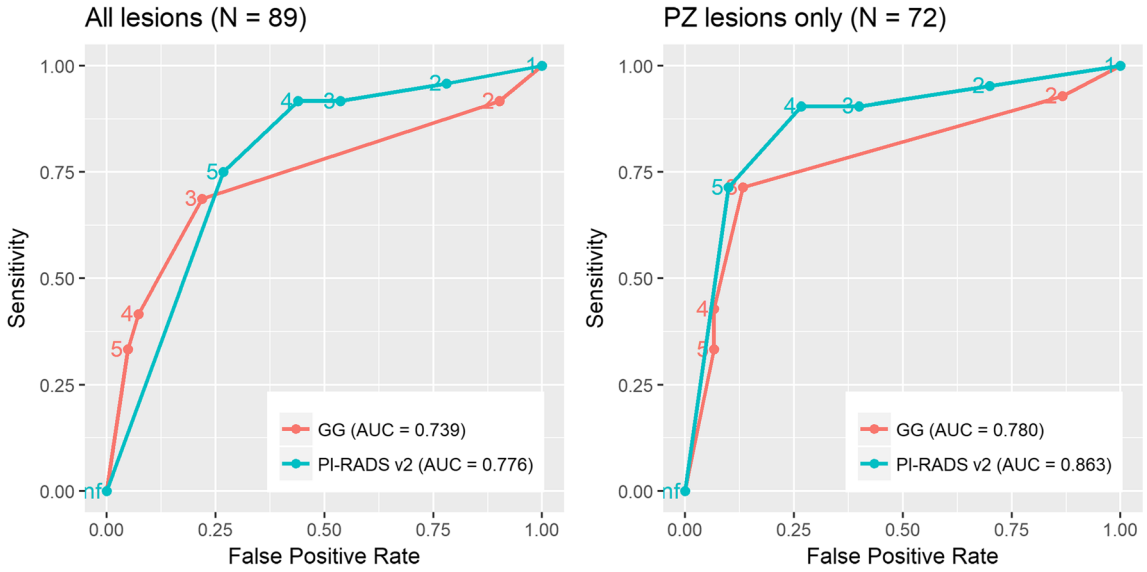

Fig. 5 ROC curves for distinguishing between low-risk lesions (Decipher score < 0.45) and intermediate-/high-risk lesions (Decipher score ≥ 0.45). The labels for the operating points indicate the associated thresholds (i.e., the operating point plots the sensitivity and false-positive rate when scores greater than or equal to the number listed are considered positive). In distinguishing between Decipher low-risk and intermediate-/high-risk lesions, the AUC for PI-RADS v2 score was slightly higher than the AUC for GG (95% CI for difference − 0.06, 0.13; $p = 0.446$). For lesions located in the PZ only, the AUC for PI-RADS v2 scores was significantly higher than the AUC for GG (95% CI for difference 0.01, 0.15; $p = 0.018$)

RP specimens [29]. The concordance was lower between index lesions and nonindex lesions (25–50%), reinforcing the existence of a substantial genomic heterogeneity in PCa even within the same patient [30].

In our study, PI-RADS v2 score was more highly correlated with Decipher risk group than with location, index status, or GG. PI-RADS v2 also demonstrated good accuracy in distinguishing between low-risk and intermediate-/high-risk lesions. The correlation and accuracy of PI-RADS v2 scores were even higher for lesions in the PZ, outperforming the accuracy of GG. These preliminary results support the use of MRI as a triage method before biopsy to reduce the detection of tumors with a low risk for progression and to assist in the sampling of lesions that may carry a high-risk genomic profile. Interestingly, however, 17.4% of MRI-invisible tumor samples in our study had Decipher scores in the intermediate-/high-risk range, suggesting that not all MRI-invisible lesions have indolent biological potential. This observation is consistent with previous research demonstrating that a subset of low-risk tumors as defined by clinicopathologic features harbor molecular features of aggressive disease [25, 31].

The strengths of this study were the uniform handling and expert pathological analysis of the RP specimens, the relatively large number of lesions analyzed, and the direct coregistration of MRI and digitally reconstructed whole-mount RP specimens, which allowed us to confidently determine the locations from which the samples sent for genomic analysis were obtained. However, this study was limited by its retrospective, single-center design. While prostate cancer is often multifocal, our study was also limited to the evaluation of a single tumor in most patients. We also acknowledge that, despite efforts to blind the radiologists to the clinicopathologic data, the inclusion of a high percentage of patients with locally advanced PCa in our cohort, especially in group 2, may have affected MRI performance. Nevertheless, this was mitigated by the inclusion of MRI-invisible lesions, which represented 25.8% of all tumors evaluated in this study. Finally, although PI-RADS v2 has been considered the reference standard in clinical practice since its inception in 2014, it is based on a qualitative assessment of MRI features and is therefore subject to interreader variability, even among experts [32]. We are working to address this limitation by evaluating the correlation between genomic expression and a set of quantitative features derived from individual MRI sequences, a process known as "radiogenomics" [33]. In our future work, we hope to use this process to identify more accurate imaging signatures of lesions with a high risk for metastases based on a stronger correlation with genomic expression analysis.

In summary, MRI phenotypes of PCa as determined by PI-RADS v2 are correlated with scores obtained from the Decipher Genomic Classifier, especially in lesions located in the PZ. These preliminary results suggest that PI-RADS v2 scores may aid in the detection of lesions with the biological potential to lead to metastatic disease based on their genomic profile. Because of the genomic heterogeneity of PCa, MRI is likely to play a synergistic role with genomic profiling.

Acknowledgements We are grateful for the editorial assistance of Megan M. Griffiths, scientific writer for the Imaging Institute, Cleveland Clinic, Cleveland, OH.

Funding This study has received funding from the Center for Clinical Genomics, Cleveland Clinic; Research Seed Grant Award Presented by

Philips/Radiological Society of North America Research & Education Foundation; and GenomicDx Biosciences.

Compliance with ethical standards

Guarantor The scientific guarantor of this publication is Andrei S. Purysko, MD.

Conflict of interest The authors of this manuscript declare relationships with the following companies: Elai Davicioni, Christine Buerki, and Marguerite du Plessis are employees of GenomeDx Biosciences.

The other authors of this manuscript declare no relationships with any companies, whose products or services may be related to the subject matter of the article.

Statistics and biometry The co-author Jennifer Bullen is a biostatistician of the Quantitative Health Sciences Department at Cleveland Clinic. She kindly provided statistical advice for this manuscript.

Informed consent Written informed consent was waived by the Institutional Review Board due to the minimal risk and retrospective nature of this study.

Ethical approval Institutional Review Board approval was obtained.

Methodology
- Retrospective
- Diagnostic or prognostic study
- Performed at one institution

References

1. Siegel RL, Miller KD, Jemal A (2018) Cancer statistics, 2018. CA Cancer J Clin 68:7–30
2. Carroll PH, Mohler JL (2018) NCCN guidelines updates: prostate cancer and prostate cancer early detection. J Natl Compr Canc Netw 16:620–623
3. Moschini M, Spahn M, Mattei A, Cheville J, Karnes RJ (2016) Incorporation of tissue-based genomic biomarkers into localized prostate cancer clinics. BMC Med 14:67
4. Erho N, Crisan A, Vergara IA et al (2013) Discovery and validation of a prostate cancer genomic classifier that predicts early metastasis following radical prostatectomy. PLoS One 8:e66855
5. Karnes RJ, Bergstralh EJ, Davicioni E (2013) Validation of a genomic classifier that predicts metastasis following radical prostatectomy in an at risk patient population. J Urol 190:2047–2053
6. Klein EA, Yousefi K, Haddad Z et al (2015) A genomic classifier improves prediction of metastatic disease within 5 years after surgery in node-negative high-risk prostate cancer patients managed by radical prostatectomy without adjuvant therapy. Eur Urol 67:778–786
7. Siddiqui MM, Rais-Bahrami S, Turkbey B et al (2015) Comparison of MR/ultrasound fusion-guided biopsy with ultrasound-guided biopsy for the diagnosis of prostate cancer. JAMA 313:390–397
8. Ahmed HU, El-Shater Bosaily A, Brown LC et al (2017) Diagnostic accuracy of multi-parametric MRI and TRUS biopsy in prostate cancer (PROMIS): a paired validating confirmatory study. Lancet 389:815–822
9. Kasivisvanathan V, Rannikko AS, Borghi M et al (2018) MRI-targeted or standard biopsy for prostate-cancer diagnosis. N Engl J Med 378:1767–1777
10. Borofsky S, George AK, Gaur S et al (2018) What are we missing? False-negative cancers at multiparametric MR imaging of the prostate. Radiology 286:186–195
11. Rosenkrantz AB, Mendrinos S, Babb JS, Taneja SS (2012) Prostate cancer foci detected on multiparametric magnetic resonance imaging are histologically distinct from those not detected. J Urol 187:2032–2038
12. Johnson DC, Raman SS, Mirak SA et al (2018) Detection of individual prostate cancer foci via multiparametric magnetic resonance imaging. Eur Urol. https://doi.org/10.1016/j.eururo.2018.11.031
13. Dianat SS, Carter HB, Pienta KJ et al (2015) Magnetic resonance-invisible versus magnetic resonance-visible prostate cancer in active surveillance: a preliminary report on disease outcomes. Urology 85:147–153
14. Ho R, Siddiqui MM, George AK et al (2016) Preoperative multiparametric magnetic resonance imaging predicts biochemical recurrence in prostate cancer after radical prostatectomy. PLoS One 11:e0157313
15. Park SY, Oh YT, Jung DC et al (2016) Prediction of biochemical recurrence after radical prostatectomy with PI-RADS version 2 in prostate cancers: initial results. Eur Radiol 26:2502–2509
16. Shiradkar R, Ghose S, Jambor I et al (2018) Radiomic features from pretreatment biparametric MRI predict prostate cancer biochemical recurrence: preliminary findings. J Magn Reson Imaging 48:1626–1636
17. Weinreb JC, Barentsz JO, Choyke PL et al (2016) PI-RADS prostate imaging—reporting and data system: 2015, version 2. Eur Urol 69:16–40
18. Penzias G, Janowczyk A, Singanamalli A et al (2016) AutoStitcher: an automated program for efficient and robust reconstruction of digitized whole histological sections from tissue fragments. Sci Rep 6:29906
19. Li L, Pahwa S, Penzias G et al (2017) Co-registration of ex vivo surgical histopathology and in vivo T2 weighted MRI of the prostate via multi-scale spectral embedding representation. Sci Rep 7:8717
20. Freedland SJ, Choeurng V, Howard L et al (2016) Utilization of a genomic classifier for prediction of metastasis following salvage radiation therapy after radical prostatectomy. Eur Urol 70:588–596
21. Obuchowski NA (1997) Nonparametric analysis of clustered ROC curve data. Biometrics 53:567–578
22. Karnes RJ, Choeurng V, Ross AE et al (2018) Validation of a genomic risk classifier to predict prostate cancer-specific mortality in men with adverse pathologic features. Eur Urol 73:168–175
23. Spratt DE, Dai DLY, Den RB et al (2018) Performance of a prostate cancer genomic classifier in predicting metastasis in men with prostate-specific antigen persistence postprostatectomy. Eur Urol 74:107–114
24. Spratt DE, Yousefi K, Deheshi S et al (2017) Individual patient-level meta-analysis of the performance of the decipher genomic classifier in high-risk men after prostatectomy to predict development of metastatic disease. J Clin Oncol 35:1991–1998
25. Klein EA, Santiago-Jiménez M, Yousefi K et al (2017) Molecular analysis of low grade prostate cancer using a genomic classifier of metastatic potential. J Urol 197:122–128
26. Den RB, Yousefi K, Trabulsi EJ et al (2015) Genomic classifier identifies men with adverse pathology after radical prostatectomy who benefit from adjuvant radiation therapy. J Clin Oncol 33:944–951

27. Li P, You S, Nguyen C et al (2018) Genes involved in prostate cancer progression determine MRI visibility. Theranostics 8: 1752–1765
28. Beksac AT, Cumarasamy S, Falagario U et al (2018) Multiparametric magnetic resonance imaging features identify aggressive prostate cancer at the phenotypic and transcriptomic level. J Urol 200:1241–1249
29. Radtke JP, Takhar M, Bonekamp D et al (2018) Transcriptome wide analysis of magnetic resonance imaging-targeted biopsy and matching surgical specimens from high-risk prostate cancer patients treated with radical prostatectomy: the target must be hit. Eur Urol Focus 4:540–546
30. Boutros PC, Fraser M, Harding NJ et al (2015) Spatial genomic heterogeneity within localized, multifocal prostate cancer. Nat Genet 47:736–745
31. Cooperberg MR, Erho N, Chan JM et al (2018) The diverse genomic landscape of clinically low-risk prostate cancer. Eur Urol 74: 444–452
32. Rosenkrantz AB, Ginocchio LA, Cornfeld D et al (2016) Interobserver reproducibility of the PI-RADS version 2 lexicon: a multicenter study of six experienced prostate radiologists. Radiology 280:793–804
33. Stoyanova R, Pollack A, Takhar M et al (2016) Association of multiparametric MRI quantitative imaging features with prostate cancer gene expression in MRI-targeted prostate biopsies. Oncotarget 7:53362–53376